ELSEVIER

Catalysis Today 58 (2000) 263–269

CATALYSIS TODAY

www.elsevier.com/locate/cattod

Fe–Co based metal/spinel to produce light olefins from syngas

F. Tihay[a], A.C. Roger[a], A. Kiennemann[a,*], G. Pourroy[b,1]

[a] *LERCSI ECPM UMR CNRS 7515, 25, Rue Becquerel, 67087 Strasbourg, France*

[b] *IPCMS UMR CNRS, 23, Rue du Loess, 67037 Strasbourg, France*

Abstract

New metal/oxide (Co–Fe) catalysts (with no reduction or thermal pre-treatment) are efficient to produce light hydrocarbons with a low selectivity in CO_2 by the Fischer–Tropsch synthesis. The low selectivity in CO_2 is due to the occurrence of the CO_2/H_2 reaction. These materials are stable under reaction conditions, and only few carbides are formed during the Fischer–Tropsch reaction. X-ray analyses indicate that the most degraded phase is the (Co–Fe) alloy phase in CO/H_2 reaction and the spinel phase in the CO_2/H_2 reaction. It was demonstrated that these composites do not behave as the simple sum of a spinel phase and a (Co–Fe) alloy but have their own properties.

Keywords: Fischer–Tropsch; Spinel; CO_2; Cobalt; Iron

1. Introduction

The profitability of the Fischer–Tropsch (F–T) technology as an industrial process to produce liquids or high-price products from syngas has been recently demonstrated [1]. Catalysts used for the F–T process are generally based on iron or cobalt, i.e. Fe/Cu/K [2] oxides or iron and/or cobalt oxide supported on alumina [3] or silica [4]. However, the crucial problems of these catalysts are on the one side the carbon formation which causes the break up of the catalysts [5], and on the other side, their attrition due to carbide formation [6]. It has been shown that the Fe_2MnO_4 [7] spinel is efficient to reduce these phenomena and Co/MnO catalysts (issued from spinel reduction) have been used for the F–T reaction [8,9]. As for us, we have successfully tested Co/Fe based materials containing a spinel phase (cobalt ferrite) and a metal phase (Co–Fe alloy) for producing light olefins from CO/H_2 [10,11]. The catalysts synthesis is based on the $Fe(OH)_2$ disproportionation into Fe_3O_4 and Fe^0 in a high basic solution. Furthermore, if Co(II) is added in the medium, the redox reaction between Co^{2+} and Fe^0 occurs: $Co^{2+}+Fe^0 \rightarrow Co^0+Fe^{2+}$. Metal iron which does not react forms a (Co–Fe) alloy. The Co(II) is involved by dehydration of hydroxide into the spinel which leads to $Co_xFe_{3-x}O_4$ with $x<1$. Then, the following material $(Co_\alpha{}^0Fe_{1-\alpha}{}^0)_\gamma[Co_xFe_{3-x}O_4]$ was synthesized [12]. In order to demonstrate that our catalysts are not a direct sum of a metallic phase and a spinel phase and in order to study their stability towards carbide formation and reducibility, their reactivity under CO_2/H_2 will be compared to that of $CoFe_2O_4$ and Co–Fe alloy. Furthermore, the contribution of the CO_2/H_2 reaction to the F–T synthesis will be discussed.

2. Experimental

In order to synthesize the catalysts, iron(II) and cobalt(II) chloride solutions were prepared with vari-

* Corresponding author. Tel.: +33-388-1369-73; fax: +33-388-1369-75.
E-mail address: kiennemann@chimie.u-strasbg.fr (A. Kiennemann)
[1] Co-corresponding author.

0920-5861/00/$ – see front matter
PII: S0920-5861(00)00260-1

ous Co to Fe ratios of 0.25, 0.33, 0.50 and 0.66. Each solution was added to a 10 M boiling KOH solution. The mixture was stirred for 1 h at constant temperature (T=115°C). The solution was filtered, and the obtained precipitate was washed with water, alcohol and then dried at 40°C for 4 h. The materials are named samples A to D for Co to Fe ratios of 0.25, 0.33, 0.50 and 0.66, respectively. $CoFe_2O_4$ has been synthesized by a classic method with Co(II) and Fe(III) chlorides precursors into KOH solution. Co–Fe alloy has been prepared by reduction of the obtained spinel in H_2 at 300°C.

The morphology of catalysts was studied by scanning electron microscopy (SEM) on a JEOL scanning electron microscope. The microstructure was observed by high resolution transmission electron microscopy (HRTEM) on a Topcon 002B microscope operating at 200 kV. Energy dispersive X-ray spectroscopy (EDXS) was used to determine the cobalt to iron ratio in the powder and the individual grain compositions. X-ray diffraction data were collected at room temperature using a D500 Siemens diffractometer equipped with a quartz monochromator (Co K_{α_1}=1.78897 Å).

Catalytic tests under CO/H_2 were performed in a fixed bed reactor with a 1 MPa pressure. 300 mg (0.2–10 μm) of catalyst was heated up to 220°C (0.2°C min^{-1}) under a 2.3 l h^{-1} nitrogen flow. Then the N_2 was replaced by the CO/H_2 (1:1) mixture with a GSHV of 3000 h^{-1}. The catalytic tests were carried out between 230 and 260°C, 60 h for each temperature.

Two types of reaction under CO_2/H_2 were carried out. The former in a small U quartz reactor at atmospheric pressure with 200 mg of catalyst and the latter in a fixed bed reactor with a 1 MPa pressure and 300 mg. In both cases, the catalyst was heated under argon (40 ml min^{-1}) up to 300°C (1°C min^{-1}). At this temperature, Ar was replaced by H_2 (20 ml min^{-1}) for 30 min. For the atmospheric pressure reaction, the CO_2/H_2 mixture (5:20 ml min^{-1}) was introduced and the temperature was rapidly increased up to 320°C. For the reaction at 1 MPa pressure, the reaction procedures were the same as the reaction at atmospheric pressure, except for the composition of the CO_2/H_2 mixture (7.5:30 ml min^{-1}). For both reactions, the outlet gases were analyzed on-line by GC and the liquid products were collected in two traps, the first one heated at 60°C and the second one cooled at 15°C, and then analyzed by GC.

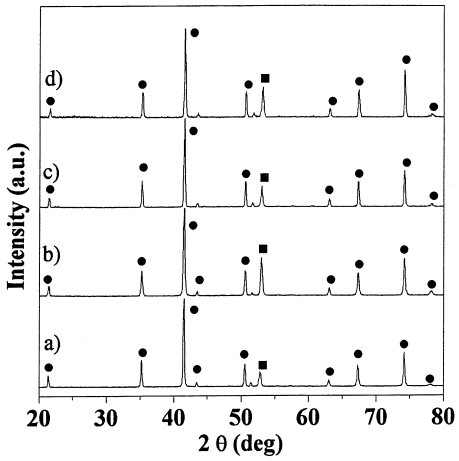

Fig. 1. X-ray diffraction patterns of samples A (a), B (b), C (c) and D (d). (●) Spinel phase, (■) Co–Fe alloy.

3. Results and discussion

3.1. Characterization of the fresh catalysts

X-ray diffraction patterns have been performed for the four catalysts (Fig. 1). The very low background indicates that the materials are well crystallized (no amorphous phase) immediately after their preparation, that is to say without any thermal treatment. The catalysts are composed of two phases: a spinel phase with a lattice parameter close to that of magnetite and cobalt ferrite, and a metallic phase, an iron–cobalt alloy of b.c.c. structure, whose of which composition is related to the lattice parameter. Catalyst A: 8.3974 (11) Å, catalyst B: 8.3990 (11) Å, catalyst C: 8.4036 (6) Å, catalyst D: 8.4058 (33) Å, these four lattice parameters are widely different from lattice parameter of Co_3O_4 from to those of $CoFe_2O_4$ and Fe_3O_4. Hence we can exclude the presence of these phases in our composite materials. Furthermore, we can note that these lattice parameters do not respect the Vegard law, since synthesis conditions, particularly the temperature, permit an augmentation of the cell volume [13]. Thus, the preparation based on the Fe^{2+} disproportionation in highly basic medium leads to materials containing

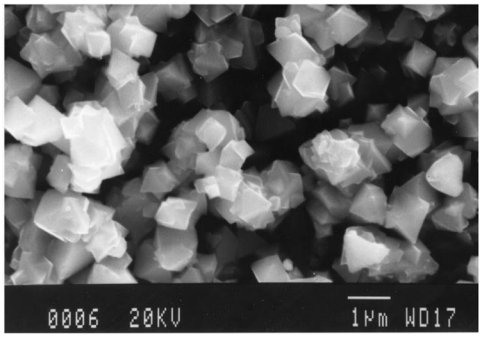

Fig. 2. Secondary SEM micrograph of fresh catalyst B.

two well-crystallized phases (oxide and metal) without thermal or reducing treatment.

SEM observations (Fig. 2) show that these materials are made of submicronic octahedral particles between 0.5 and 1 μm. Thermal gravimetric analysis in air shows that they do not oxidize below 150°C, thus these materials are stable in air. The TEM observation presented in Fig. 3 shows that both phases are well fitted into each other. The metal grains are about 50–150 nm wide. They are often located close to the surface, their outer surface being coated by an amorphous or a poorly crystallized oxide or hydroxide layer which protects them from oxidation [14]. Such materials are composite materials. By means of EDXS, thermal gravimetric analyses and the value of the metallic phase lattice parameters, the formulae of the four catalysts were determined [11]:

A (Co/Fe bulk ratio=0.23): $(Co_{0.61}Fe_{0.39})_{0.69}[Co_{0.27}Fe_{2.73}O_4]$,

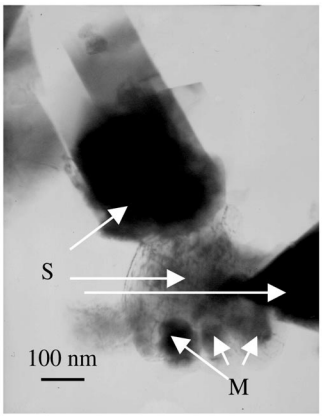

Fig. 3. TEM micrograph. S: spinel phase and M: Co–Fe alloy.

B (Co/Fe bulk ratio=0.33): $(Co_{0.61}Fe_{0.39})_{0.84}[Co_{0.41}Fe_{2.59}O_4]$,

C (Co/Fe bulk ratio=0.45): $(Co_{0.73}Fe_{0.27})_{0.58}[Co_{0.69}Fe_{2.31}O_4]$,

D (Co/Fe bulk ratio=0.53): $(Co_{0.71}Fe_{0.29})_{0.87}[Co_{0.72}Fe_{2.28}O_4]$.

The loss of cobalt during the preparation with respect to the theoretical Co/Fe ratios in the chloride solutions can be explained by the nonzero solubility of $Co(OH)_2$ in highly basic medium. From the formulae of the four catalysts, it can be concluded that the increase of the Co to Fe ratios in the chloride solutions results in a higher cobalt to iron ratio in the spinel from 0.27 to 0.72 for cobalt, while it has only few effects on the alloy composition from 0.61 to 0.73 for cobalt. However, we observe a variation of the amount of metal phase which does not vary linearly with the bulk Co/Fe ratios.

As a summary, the catalysts A, B, C and D, contain two well fitted into each other crystallized phases, are composite materials and are stable in air. They are very different from impregnated catalysts and are not issued from conventional reduction of spinels.

3.2. Catalytic tests under CO/H_2

The catalysts were tested for the F–T synthesis, and results are presented in Table 1 at iso-conversion of CO of almost 5%.

As regards to the C_2–C_4 olefins production, catalyst C is the best catalyst. Indeed, the hydrocarbon (HC) molar selectivity is high (84.8%). The C_2–C_4 fraction represents 47.8% in weight of total hydrocarbons with a olefin/paraffin (O/P) ratio of 3.7 in this fraction. Catalysts B and D present similar catalytic behavior but are less selective in olefins and produce more CO_2 (23.6 and 21.6%, respectively, compared to 15.2% for C). Catalysts C and D are composed of the same two phases (same spinel, same alloy), only their metal/spinel ratio is different. Catalyst C contains 12.5 wt.% of alloy, while catalyst D contains 17.8 wt.% of alloy. So a high amount of metal seems to have a negative effect on the olefin production, on the overall hydrocarbon selectivity and on the O/P ratio in the C_2–C_4 fraction. This is confirmed by the behavior of catalyst B which contains 17.3 wt.% of alloy. Catalyst A behaves very differently. Although the CO_2 production is quite low (18.4% molar

Table 1
Results of CO/H_2 reaction of catalysts (A to D) at iso-conversion of CO

	Catalysts			
	A	B	C	D
Co/Fe ratio	0.23	0.33	0.45	0.53
Temperature (°C)	250	240	250	250
Total CO conversion (%)	5.9	5.1	5.2	6.2
Molar selectivity (%) of				
CO_2	18.4	23.6	15.2	21.5
Gaseous hydrocarbons	35.6	49.4	61.7	56.2
Liquid hydrocarbons	46.0	27.0	23.1	22.3
Hydrocarbons distribution (wt.%) in the gaseous fraction C_1–C_4				
C_1	34.9	32.6	34.3	36.5
C_2; $C_2^=$	9.7; 14.1	9.4; 9.7	5.9; 12.4	7.1; 4.2
C_3; $C_3^=$	3.9; 23.9	4.6; 19.9	4.1; 20.7	4.7; 25.3
C_4; $C_4^=$	2.8; 10.7	6.3; 17.3	4.0; 18.5	4.9; 17.3
Total C_2–C_4	65.1	67.4	65.7	63.5
Olefin to paraffin ratio in the C_2–C_4 fraction	3.0	2.3	3.7	2.8
Percentage of olefins in the C_2–C_4 fraction	75	70	79	74

selectivity), the selectivity to C_2–C_4 olefins is low since more liquid hydrocarbons are produced (46.0% molar selectivity with a growing chain up to 40 carbons compared to 22–27% for the other catalysts with a growing chain less than 10 carbons).

After CO/H_2 reaction, the four systems were then studied by XRD. The X-ray diffraction patterns are presented in Figs. 4 and 5. Except for catalyst B, the systems undergo very weak changes (Fig. 4) during the F–T reaction (~200 h). In all cases the spinel phase is still present and the composition of the alloy remains unchanged. χ-Fe_5C_2 (Hagg Carbide) and Co_2C are the carbide phases detected in catalysts A and D after test, Co_2C is the only carbide phase found in catalyst C. Co_2C was previously observed by Ducreux et al. [15] with Co–SiO_2 catalysts. The ratios of the integrated

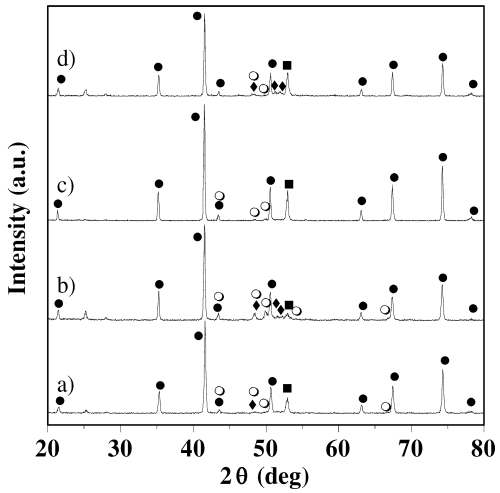

Fig. 4. X-ray diffraction patterns (2θ range 20–80°) after CO/H_2 reaction of the catalysts A (a), B (b), C (c) and D (d). (●) Spinel phase, (■) Co–Fe alloy, ○ Co_2C, ◆ χ-Fe_5C_2.

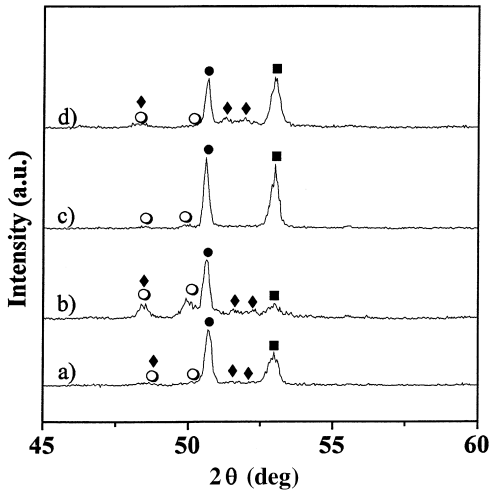

Fig. 5. X-ray diffraction patterns (2θ range 45–60°) after CO/H_2 reaction of the catalysts A (a), B (b), C (c) and D (d). (●) Spinel phase, (■) Co–Fe alloy, (○) Co_2C, (◆) χ-Fe_5C_2.

Table 2
Ratio of the integrated intensity of the diffraction lines (1 1 0) of (Co–Fe) alloy and (3 1 1) of the spinel[a]

	Catalyst			
	A	B	C	D
R1 fresh catalyst	17.0/100	43.0/100	24.0/100	34.0/100
R2 after CO/H_2 reaction	17.0/100	8.0/100	26.0/100	28.0/100
R2/R1	1.0	0.2	1.1	0.8
R3/R1	1.3	3.9	1.3	1.3

[a] R1: ratio of the integrated intensity of the diffraction lines (1 1 0) of (Co–Fe) alloy and (3 1 1) of the spinel before test; R2: Ratio of the integrated intensity of the diffraction lines (1 1 0) of (Co–Fe) alloy and (3 1 1) of the spinel after CO/H_2 reaction; R3: Ratio of the integrated intensity of the diffraction lines (1 1 0) of (Co–Fe) alloy and (3 1 1) of the spinel after CO_2/H_2 reaction.

intensity of the diffraction line (1 1 0) of the (Co–Fe) alloy and the integrated intensity of the diffraction line (3 1 1) of the spinel are presented in Table 2 for fresh catalysts (R1) and for the catalysts after CO/H_2 reaction (R2). The relative stability of the two phases can be deduced from R2/R1 ratios. A low R2/R1 ratio means that either the (Co–Fe) alloy concentration has decreased and the spinel has been preserved, or both are transformed but the (Co–Fe) alloy much more than the spinel phase. For catalyst B, R2/R1=0.2 which corresponds to a quite total transformation of the metal phase. For catalysts A, C and D the R2/R1 ratios are, respectively, 1.0, 1.1 and 0.8, which means that these three catalysts are stable. This is in good agreement with the few amount of carbides detected after tests on catalysts A, C and D (Fig. 5).

3.3. Catalytic tests under CO_2/H_2

In order to understand the stability of our catalysts towards carbide formation and reducibility, and to explain the various CO_2 selectivities, their reactivity under CO_2/H_2 was studied and compared to that of $CoFe_2O_4$ and the Fe–Co alloy.

Contrary to CO/H_2 reaction, the catalysts were pretreated under H_2 for 30 min at 300°C. By X-ray diffraction analysis, neither a spinel reduction nor a variation of the alloy lattice parameter have been observed.

All the studied catalysts (A, B, C, D, (Co–Fe) alloy and $CoFe_2O_4$) are active to reduce CO_2 into CO and

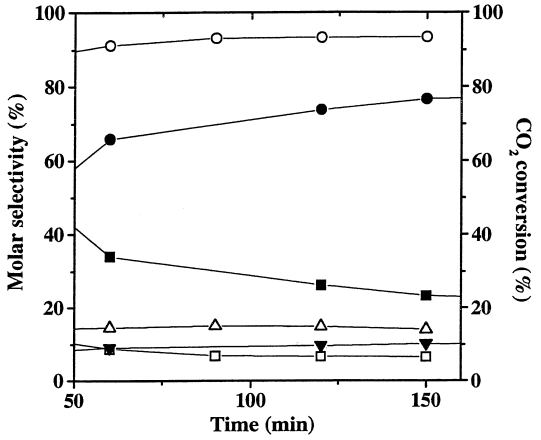

Fig. 6. CO_2 conversion at atmospheric pressure for catalyst C. At 260°C: molar selectivity in CH_4 (■), CO (●) and CO_2 conversion (▼). At 320°C: molar selectivity in CH_4 (□), CO (○) and CO_2 conversion (△).

CH_4 at atmospheric pressure. Fig. 6 presents the CO and CH_4 selectivities obtained on catalyst C at 260 and 320°C. One hour of reactivity is necessary to reach the steady state. It must be noted that, contrary to Ni-based catalysts [16,17], CO is the major reaction product. It clearly appears that the CO selectivity increases with temperature and CO_2 conversion.

The CO_2 conversion versus time at 320°C at atmospheric pressure is given in Fig. 7 for A, B, C, D, $CoFe_2O_4$ and (Co–Fe) alloy. For $CoFe_2O_4$, the CO_2 conversion is maximal and equal at 22% after 6 h, then it begins to decrease. X-ray characterization after test (Fig. 8a) indicates that the spinel is almost completely transformed into χ-Fe_5C_2, Co_2C and probably a cobalt rich Fe–Co alloy. The (Co–Fe) alloy reaches a maximal activity of 20% after 75 min and then it rapidly deactivates. X-ray diffraction pattern (Fig. 8b) reveals the presence of the same phases as for $CoFe_2O_4$. The increasing activity of spinel may be due to continuous spinel reduction, the deactivation being due to the increasing formation of carbides via carbon deposition. Iron carbides formation would also be the reason why the (Co–Fe) alloy catalyst deactivates.

All the catalysts A, B, C and D deactivate with time, the deactivation being more pronounced for catalyst B. The deactivation slopes (CO_2 conversion (%) min^{-1}) for CO_2 conversion have been calculated and are in the order: Fe–Co alloy (-202) > B(-134) > A(-57) ∼ C(-55) ∼ D(-59).

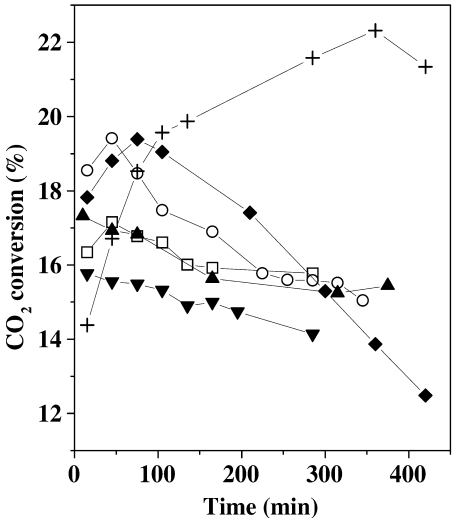

Fig. 7. CO_2 conversion at atmospheric pressure at 320°C: for catalysts A (□), B (○), C (▲), D (▼), Co–Fe (◆) alloy and $CoFe_2O_4$ (+).

X-ray diffraction patterns performed on A, B, C and D catalysts (Fig. 8c for catalyst D) after CO_2/H_2 indicate that only few carbides are formed, as previously observed after CO/H_2 reaction. The ratios R3 of the integrated intensity diffraction lines (as in 3.2) have been calculated after CO_2/H_2 reaction (Table 2). The ratio R3/R1 is 3.9 for catalyst B while it takes the same value (1.3) for the three other catalysts. Contrary to what is observed after CO/H_2 reaction, the spinel phase is more degraded than the alloy phase.

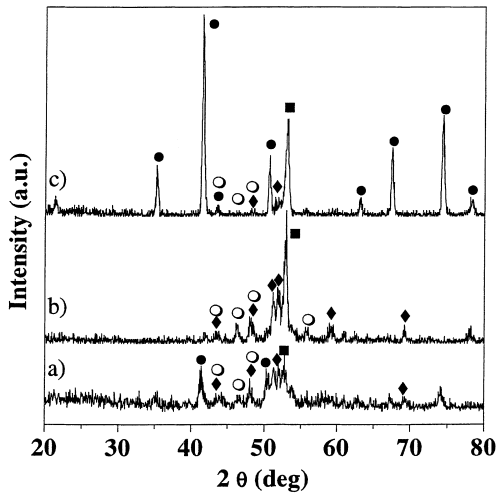

Fig. 8. X-ray diffraction patterns after CO_2/H_2 reaction of $CoFe_2O_4$ (a), Co–Fe alloy (b) and catalyst D (c). (●) Spinel phase, (■) Co–Fe alloy, (○) Co_2C, (◆) χ-Fe_5C_2.

The reactivity of catalyst A was studied at 1 MPa pressure. At 300°C, catalyst A converts 42% of CO_2 with a hydrocarbon selectivity of 82%. The C_2–C_4 fraction represents almost 42% (wt.%) of the hydrocarbons, and the O/P ratio in this fraction is 1.2. These results compete with those obtained with the best catalysts (K–Fe–Mn based catalysts) studied by Longya et al. [18]. It appears that this catalyst is very efficient for the production of light olefins from CO_2 hydrogenation. After reaction, X-ray diffraction pattern show that the catalyst A presents the same evolution than under CO_2/H_2 reaction at atmospheric pressure.

It can be concluded that our materials do not behave as a simple sum of a spinel phase and a (Co–Fe) alloy, but have their own catalytic behavior and present much higher stability than $CoFe_2O_4$ or (Co–Fe) alloy alone. It must be remembered that for the F–T reaction, the order of stability of the catalysts was B<A∼C∼D. Thus, the CO_2/H_2 reaction could be considered as a reaction test to predict the stability of the catalysts under CO/H_2. By comparing the CO_2 selectivities obtained in the F–T reaction for catalysts A, B, C and D (18.4, 23.6, 15.2 and 21.5%, respectively) to the values of R2/R1 for each catalyst (1.0, 0.2, 1.1 and 0.8, respectively), it can be seen that these two parameters vary in the same order. Catalyst B is the catalyst which produces more CO_2, this is in agreement with the low value of R2/R1, which indicates that the CO_2/H_2 reaction did not occur during the F–T synthesis. Catalyst C produces only 15.2% of CO_2, its R2/R1 value is 1.1, this indicates that CO_2/H_2 reaction occurred during the F–T reaction. Therefore, the R2/R1 value is a parameter accounting for the participation of the CO_2/H_2 reaction to the F–T synthesis.

4. Conclusion

The synthesis based on Fe^{2+} disproportionation in highly basic medium leads to well-crystallized metal/oxide composite materials ($(Co_\alpha{}^0Fe_{1-\alpha}{}^0)_\gamma$ $[Co_xFe_{3-x}O_4]$) without thermal nor reducing treatment.

These catalysts are efficient to produce C_2–C_4 olefins from CO/H_2. The Co/Fe ratio of the systems has an effect on the reactivity, the best ratio being 0.5. These composite materials are stable under CO/H_2 and after a reaction time of 200 h only few carbides are detected.

The reactivity under CO_2/H_2 seems to provide a good prediction of the stability of the systems under CO/H_2. XRD analyses show that the most degraded phase is: (i) the (Co–Fe) alloy phase in the case of CO/H_2 conditions (R2/R1=0.2 for catalyst B) and (ii) the spinel phase in the case of CO_2/H_2 conditions (R3/R1=3.9 for catalyst B).

It has been shown that our materials do not consist of a simple addition of the two component phases, since the composite character stabilizes the catalysts towards carbide formation and reduction.

References

[1] M.J. Gradassi, Stud. Surf. Sci. Catal. 119 (1998) 35.
[2] Z.-T. Liu, Y.-W. Li, J.-L. Zhou, B.-J. Zhang, J. Chem. Soc. Faraday Trans. 91 (1995) 3255.
[3] M.K. Niemelä, L. Backman, A.O.I. Krause, T. Vaara, Appl. Catal A 156 (1997) 31.
[4] D. Schanke, A.M. Hilmen, E. Bergene, K. Kinnari, E. Rytter, E. Adnanes, A. Holmen, Energy Fuel 10 (1996) 868.
[5] B. Jager, Stud. Surf. Sci. Catal. 119 (1998) 35.
[6] M.D. Shroff, D.S. Kalakkad, M.S. Harrington, N.B. Jackson, K.E. Coulter, A.G. Sault, A.K. Datye, in: Chapman, et al. (Eds.), The Chemistry of Transition Metal Carbides and Nitrides, 1995, p. 520 (Chapter 28).
[7] C.H. Bartholomew, in: L. Guczi (Ed.), Trends in CO Activation, Elsevier, Amsterdam, 1991 (Chapter 5).
[8] A.A. Adesina, Appl. Catal. 138 (1996) 345.
[9] G.J. Hutchings, R.G. Copperthwaite, M. Van der Riet, Topics Catal. 2 (1995) 163.
[10] C. Cabet, A.C. Roger, A. Kiennemann, S. Läkamp, G. Pourroy, J. Catal. 173 (1998) 64.
[11] F. Tihay, A.C. Roger, G. Pourroy, A. Kiennemann, Stud. Surf. Sci. Catal. 119 (1998) 143.
[12] S. Läkamp, A. Malats i Riera, G. Pourroy, P. Poix, J.-L. Dormann, J.-M. Greneche, Eur. J. Solid State Inorg. Chem. 32 (1995) 159.
[13] S. Läkamp, G. Pourroy, Eur. J. Solid State Chem. 34 (1997) 295.
[14] J.C. Yamegni-Noubeyo, G. Pourroy, J. Werckmann, A. Malats i Riera, G. Ehret, P. Poix, J. Am. Ceram. Soc. 79 (1996) 2027.
[15] O. Ducreux, J. Lynch, B. Rebours, M. Roy, P. Chaumette, Stud. Surf. Sci. Catal. 119 (1998) 125.
[16] S. Komarneni, M. Tsuji, Y. Wada, Y. Tamaura, J. Mater. Chem. 7 (12) (1997) 2339.
[17] H. Kato, T. Sano, Y. Wada, Y. Tamaura, M. Tsuji, T. Tsuji, S. Miyazaki, J. Mater. Sci. 30 (1995) 6350.
[18] X. Longya, W. Qingxia, L. Dongbai, W. Xing, L. Liwu, C. Wei, X. Yide, Stud. Surf. Sci. Catal. 119 (1998) 221.